Appl Phys B (2011) 104:503–511
DOI 10.1007/s00340-011-4636-7

Applied Physics B
Lasers and Optics

Temperature induced nonlinearity in coupled microresonators

C. Schmidt · A. Chipouline · T. Käsebier · E.-B. Kley · A. Tünnermann · T. Pertsch

Received: 31 March 2011 / Revised version: 4 May 2011 / Published online: 26 July 2011

Abstract We present here, our most recent results from theoretical and experimental investigations of optical properties of coupled microresonators. While fused silica spherical microresonators with Q-factors of about 10^7 to 10^8 can be quite easily fabricated, the production of a number of equally sized spheres, which appears to be a necessary condition for effective light coupling, has proved challenging. In order to bypass this problem we focus our attention on the investigation of coupled disk microresonators made of fused silica. These may be fabricated in almost arbitrary two-dimensional configuration with nanometer precision. A Q-factor of 10^5 can be routinely achieved, which relaxes the requirements on uniformity of the microdisks to within the range of fabrication accuracy. The achieved Q-factors are high enough to observe thermal nonlinear effects in the fabricated coupled disks. A detailed experimental analysis of the thermal nonlinear resonance behavior in a system of two coupled microdisks now follows. The results were found to be in good agreement with the respective calculations based on coupled mode theory including temperature induced nonlinear response.

1 Introduction

Whispering-gallery-mode (WGM) microresonators of differing geometries (spheres [1], disks [2], toroids [3]) have attracted a great deal of interest for more than a decade, due to their extremely high Q-factors and small mode volume, which allows the investigation of various nonlinear effects at relatively low input powers. These unique properties, together with their compact size, make them attractive for potential applications in optoelectronics [4]. In addition optical microresonators provide a convenient tool for studying many fundamental phenomena, such as Raman scattering [5, 6], parametric oscillation [7], cavity quantum electrodynamic effects [8, 9], lasing [2], optomechanics [10] etc. The potential of coupling between microresonators proved particularly interesting and various aspects were investigated. Light propagation and optical coupling effects in bi-sphere systems [11] as well as in long chains of coupled microspheres [12–14] were investigated theoretically. Due to the requirement of extreme size uniformity for high-Q coupled microresonators [15], such systems were experimentally investigated, in the main, for two coupled microspheres [17]. Similarities to electromagnetic induced transparency [16] and slow light in coupled resonators [18] were observed. For systems with a large number of resonators the influence of high size disorder on the optical coupling and transport phenomena in chains of microspheres [19, 20] were investigated. Coupled disk microresonator systems usually can be fabricated with nanometer precision, which in combination with lower Q-factor in comparison to microspheres, relaxes the requirements on size uniformity. Such systems were investigated theoretically in various configurations of passive photonic molecules [21], for application as optical sensors and as active lasing elements [22]. The modes in coupled resonators were also investigated as building blocks for coupled resonator optical waveguides (CROW [23]), for optical delay lines [24] and as high-order filters [25]. The optical coupling and formation of coupled resonator eigenstates were experimentally observed for two and three coupled mi-

C. Schmidt (✉) · A. Chipouline · T. Käsebier · E.-B. Kley · A. Tünnermann · T. Pertsch
Institute of Applied Physics, Friedrich-Schiller-Universität Jena, Max-Wien-Platz 1, 07743 Jena, Germany
e-mail: ca.schmidt@uni-jena.de

A. Tünnermann
Fraunhofer Institute of Applied Optics and Precision Engineering, Albert-Einstein-Strasse 7, 07745 Jena, Germany

crodisks [26] and temperature induced optical instability in coupled microtoroids was investigated in [27].

In addition to various potential applications mentioned above, it has been recognized that the coupled optical cavities are perfect examples of discrete dissipative nonlinear systems and thus allowed us to use the microcavities as a test bed for the investigation of dissipative nonlinear dynamics. The recent unification of various physical effects under the topic of dissipative nonlinear dynamics has given new momentum for fundamental research. The existence of localized spatio-temporal structures in dissipative nonlinear systems has been proven theoretically and experimentally in a wide range of physical systems [28]. It has been shown that, in spite of the different physical nature, the systems exhibit similar dynamics, namely dynamics which allow the existence of attractors of different types. This similarity suggests the natural step that one area of complex nonlinear dynamics may be investigated using the well known tests and methods from another area. Optics in this case provides unique test bed allowing numerous different combination of loss/amplification, various types of dispersion and nonlinearities which, in turn, allows the possibility of testing various physical models using the same experimental methods.

In order to test the experimental capabilities of the coupled microdisk system to use as a test bed for discrete nonlinear dynamics, we investigated the influence of fabrication tolerance on the observed nonlinear effects. It turned out that thermal nonlinearity for the fused silica microresonators has the lowest threshold [29] and a relatively slow nonlinear response [30]. Nevertheless, it was shown that for long enough times it mimics a third order nonlinearity like Kerr effect, which is usually under investigation in other discrete nonlinear systems.

The paper is structured as follows. In Sect. 2 we present the theoretical model elaborated for the coupled microdisk resonators including temperature induced nonlinearity. In Sect. 3 the sample fabrication and measurement setup are described. Thereafter we present experimental results and discuss the observed effects (Sect. 4) for two coupled microdisks.

2 Coupled mode equations with thermal nonlinearity

As mentioned previously in Sect. 1, a coupled microdisk system is usually described in two dimensions using numerical solution of integral equations (see the recent review [31] and references therein). The reduction of dimensionality is valid as long as the disk radius is much larger than the thickness of the disk, which is usually fulfilled for the systems under investigation (see Fig. 2a for a system of two coupled silica microdisks). However, the disks used in this work have almost circular shape, which allows us to use a simpler, physically more transparent approach based on modal expansion [26]. With this approximation it becomes feasible to investigate large coupled disks (radius much larger than wavelength) in a rigorous fashion (depending of size and material parameters of the disks only) by taking into account the coupling of all disks with each other and all possible modes. For this purpose, it is usually assumed that a particular mode in one of the disks is already excited and acts as a source of excitation for all other disks and modes. As shown in [26] such assumption are sufficient for the calculation of such spectrum characteristics like resonance splitting or relative excitation strength, but fail in describing the experimental situation of excitation of the coupled disks system with a tapered optical fiber (which is the most efficient method of excitation of microresonators [32, 33]).

In order to describe the experimental situation more adequately and perform direct comparison of calculations with measured reflection and transmission data we use a different approach based on coupled mode theory [34]. As an advantage, one can easily introduce scattering losses due to surface roughness, which is not straightforward for the modal expansion method because it assumes perfect circular shaped microdisks. A consequence of surface roughness is the coupling of clockwise (cw) and counterclockwise (ccw) propagating modes in each disk due to Rayleigh scattering, leading to a resonance splitting even in a single resonator and a reflection signal in the tapered fiber used for excitation. Similarly one can introduce modifications of the mode amplitudes due to nonlinear interactions like Kerr nonlinearity and temperature induced phase shifts. Generally, the time dynamics of the slowly varying amplitudes of the clockwise (a_{cw}) and counterclockwise (a_{ccw}) propagating modes in the pth disk of an arbitrary arrangement can be described by

$$\dot{a}_{\mathrm{cw}}^{(p)}(\omega) = X^{(p)} a_{\mathrm{cw}}^{(p)} + i\,\Gamma_{\mathrm{c}}^{(p)} a_{\mathrm{ccw}}^{(p)} + i \sum_{q} \Gamma_{pq} a_{\mathrm{ccw}}^{(q)} + Y^{(p)}, \tag{1}$$

$$\dot{a}_{\mathrm{ccw}}^{(p)}(\omega) = X^{(p)} a_{\mathrm{ccw}}^{(p)} + i\,\Gamma_{\mathrm{c}}^{(p)} a_{\mathrm{cw}}^{(p)} + i \sum_{q} \Gamma_{pq} a_{\mathrm{cw}}^{(q)}, \tag{2}$$

with

$$X^{(p)} = i\,\Delta\omega^{(p)} - \Gamma_0^{(p)} - \Gamma_{\mathrm{ext}}^{(p)} + i\,\omega_0^{(p)} \beta_{\mathrm{th}} \Theta^{(p)}, \tag{3}$$

$$Y^{(p)} = i\sqrt{2\Gamma_{\mathrm{ext}}^{(p)}}\, A_{\mathrm{in}}. \tag{4}$$

Here $\Delta\omega = \omega - \omega_0$ denotes the frequency detuning of the excitation from the resonance frequency ω_0 of the disk, Γ_0 is the intrinsic energy loss rate and Γ_{ext} is the energy coupling rate. The coupling of a_{cw} and a_{ccw} mentioned above is described with the coupling rate Γ_c . The coupling to neighboring disks is accounted for with the coupling rate Γ_{pq} with the sum depending on the actual number of disks and their

arrangement. The pump through the tapered fiber was assumed to be in one direction and therefore influences the cw mode only. The mode amplitudes itself are normalized to the energy stored in the resonator ($|a_{\mathrm{cw}}|^2 + |a_{\mathrm{ccw}}|^2 = U$), whereas the amplitude of the pump field is normalized to the pump power ($|A_{\mathrm{in}}|^2 = P_{\mathrm{in}}$). Due to the fact that thermal nonlinearity has the lowest threshold in the investigated system and is much stronger than the Kerr nonlinearity, the only nonlinear term taking into account is proportional to the mean temperature difference Θ of the disk volume occupied by the mode and related to thermorefractivity and thermal expansion of the disks material,

$$\beta_{\mathrm{th}} = \left(\frac{1}{n}\frac{dn}{dT} + \frac{1}{3V}\frac{dV}{dT}\right). \tag{5}$$

The mean temperature difference of the mode volume can be written according to [35] as

$$\Theta^{(p)} = \int \left(T - T_0^{(p)}\right)\left|\mathbf{E}_0(\mathbf{r})\right|^2 d^3\mathbf{r}, \tag{6}$$

where $T_0^{(p)}$ is the temperature of the mode volume for zero input power and $\mathbf{E}_0(\mathbf{r})$ is the modes normalized spatial field distribution ($\int |\mathbf{E}_0(\mathbf{r})|^2\, d\mathbf{r} = 1$). The integration in (6) is performed over the mode volume. The temperature dynamics of the mode volume can be approximated from a heat diffusion equation by

$$\dot{\Theta}^{(p)} = -\delta_{\mathrm{th}}\Theta^{(p)} + B_{\mathrm{th}}\left(\left|a_{\mathrm{cw}}^{(p)}\right|^2 + \left|a_{\mathrm{ccw}}^{(p)}\right|^2\right), \tag{7}$$

with the absorption parameter (according to [35])

$$B_{\mathrm{th}} = \frac{\alpha c}{\rho_0 \bar{C} n V_{\mathrm{eff}}}. \tag{8}$$

Here α is the material absorption coefficient, c is the speed of light, ρ_0 is the material density, $\bar{C}$ is the materials heat capacity, n the refractive index and V_{eff} is the mode volume which usually is obtained from finite element simulations of a single disk. A crucial parameter in (7) is the thermal relaxation rate δ_{th} that depends on the present relaxation mechanism in the system. As it was discussed in [29] one usually has to deal with two different relaxation regimes. The first one is the relaxation of the accumulated heat from the mode volume to the rest of the resonator. The second is the relaxation of the heat from the whole resonator to the surrounding. Depending on the resonator geometry and the setup environment two main mechanisms of heat exchange (heat conductivity and convection) can have different contribution to the relaxation process. The heat conductivity additionally depends strongly on the resonator material but for microspheres it will have stronger contribution than for microdisks. This can be understood by the larger reservoir volume which a sphere provides for the heated mode volume (which is only a ring along the equator of the sphere) in comparison to a very thin disk (compared to its radius). If the setup is not evacuated the heat convection of the surrounding gas plays an important role. Especially, for thin microdisks with a volume to surface ratio proportional to the thickness of the disk the contact to the environment is increased in comparison to microsphere resonators, where the volume to surface ratio is proportional to the radius. Therefore, the main contribution to the temperature relaxation in the case of coupled silica disk microresonators surrounded by air comes from the heat convection and the relaxation rate can be approximated by [29]

$$\delta_{\mathrm{th}} = \frac{\bar{k}N}{\rho_0 \bar{C} R^2}. \tag{9}$$

Here $\bar{k}$ is the thermal conductivity of the disks material, N is the Nusselt number ($\approx$0.3 for air at room temperature) and R is the radius of the disk.

Equations (1), (2) and (7) describe the time evolution of modes in coupled disk microresonators including thermal nonlinearity. With the assumption that only one of the disks is coupled to the tapered fiber for pumping and signal detection, the transmission ($\mathcal{T}$) and reflection ($\mathcal{R}$) can be calculated from the transmitted (A_{tr}) and reflected (A_{rf}) fields to

$$\mathcal{T} = \left|\frac{A_{\mathrm{tr}}}{A_{\mathrm{in}}}\right|^2 = \left|1 + \frac{i\sqrt{2\Gamma_{\mathrm{ext}}}a_{\mathrm{cw}}^{(1)}}{A_{\mathrm{in}}}\right|^2, \tag{10}$$

$$\mathcal{R} = \left|\frac{A_{\mathrm{rf}}}{A_{\mathrm{in}}}\right|^2 = \left|\frac{i\sqrt{2\Gamma_{\mathrm{ext}}}a_{\mathrm{ccw}}^{(1)}}{A_{\mathrm{in}}}\right|^2. \tag{11}$$

3 Sample fabrication and setup

Coupled silica disk microresonators were fabricated by an electron-beam lithography process with subsequent etching steps. A detailed description of the basic steps illustrated in Fig. 1a can be found in [26] and [36]. For the samples investigated in this paper we made a minor modification for the removal of the silicon substrate underneath the silica layer. Replacing the inductively coupled plasma etch (ICP) with a wet-chemical potassium hydroxide (KOH) etch allows us to achieve homogeneously under-etched coupled silica disk samples. For the samples with two coupled disk used here for demonstrating thermal nonlinear effects in coupled resonators, it practically makes no difference which process is used. A comparison of the influence on the optical properties (especially the Q-factor) shows no significant difference between ICP and KOH process. In contrast, for two-dimensional coupled microdisk arrays it is essential which process is used to obtain working samples. The reactive ions

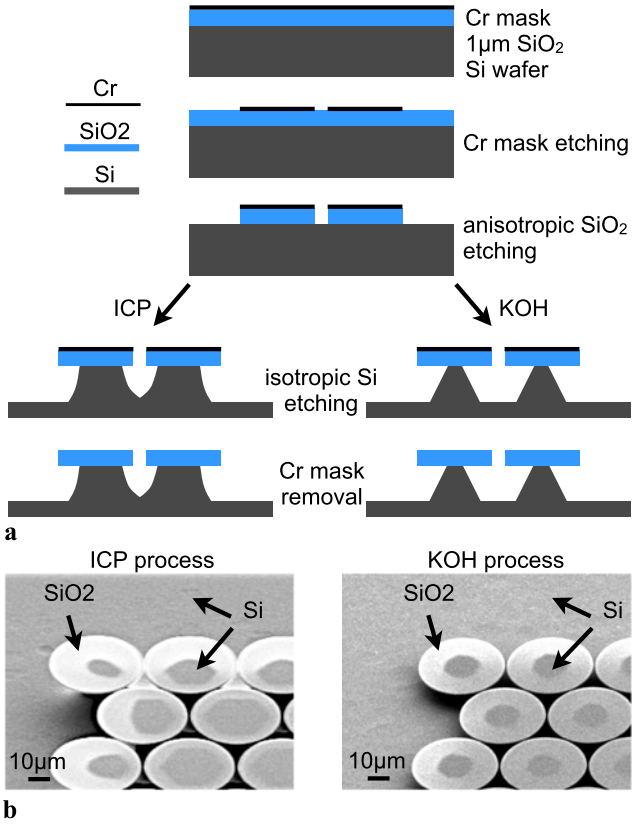

Fig. 1 Illustration of sample fabrication (**a**) and scanning electron micrograph showing the difference of inductively coupled plasma (ICP) process and wet-chemical etching (KOH) for two-dimensional arrays of coupled microdisks (**b**)

in the ICP process preferentially etch the silicon from the outside of the sample, whereas the etch ratio is reduced along the directions where the disks are coupled to each other (the disks effectively screen the substrate from the reactive ions). This leads to insufficient under-etching of disks in the center of the structure. Figure 1b illustrates the difference for the two etching methods. For the ICP process the observed silicon pedestals are small and strongly asymmetric for the outer disks and very large for the inner disks of the structure (dark gray area in each of the disks in the left picture of Fig. 1b). In comparison the wet-chemical KOH process leads to equally sized and circular shaped silicon pedestals for inner and outer disks of the structure (right picture in Fig. 1b). The obtained samples on a 1×1 cm^2 large chip show a substrate to disk distance of about 10 to 20 µm.

In the experiments a tapered optical fiber excitation scheme was used in order to efficiently couple light from a tunable laser source (Agilent 81600/81640A) to the samples and in parallel collect transmission and reflection signals modified by the spectral response of the disks. The obtained optical signals were detected by receivers with an electrical bandwidth of 125 MHz (Terahertz Technologies Inc.) and visualized by an oscilloscope (Agilent DSO 6104A). Sample and tapered fiber were housed in a clean box to prevent them from contamination of dust and environmental fluctuations. For coarse alignment both were mounted on motorized stages and for fine adjustment the tapered fiber additionally could be moved by piezo actuators. The whole coupling to the sample was controlled with a microscope setup. The samples were placed on a thermo electric cooler to stabilize their temperature during the tests and prevent them from heating up due to the motorized actuators inside the housing. Figure 2a shows the arrangement of two coupled microdisks with diameter of about 40 µm and a gap size of 300 nm coupled to a tapered optical fiber. The important variables used in the model described in Sect. 2 are highlighted. For spectrum measurements the wavelength of the laser sweeps from shorter to longer wavelengths over a certain range at a fixed sweeping speed while the transmission (reflection) through the taper can be displayed on the oscilloscope representing the spectrum of the investigated resonators.

4 Experimental characterization of two coupled disks

4.1 Linear characterization

The spectrum of the structure for a broad wavelength range in Fig. 2b shows several closely spaced doublet transmission dips, which are related to the splitting of the resonances due to the coupling between the disks. The first order radial modes (referred to as fundamental modes) additionally show a strong reflection signal that is useful for identification of the different orders of excited modes. The resonance frequencies can be fitted according to the rigorous modal expansion method [26] and the different polarization states can be identified. The fitting leads to a refractive index and thickness of the disks of $n = 1.4498$ and $d = 1.0028$ µm which is in agreement with scanning electron micrographs of the disk samples and wafer specifications.

For a detailed analysis a first order TM mode was chosen. As mentioned above the introduced loss rates in the coupled mode model have to be obtained from independent measurements. The intrinsic energy loss rate Γ_0 can be related to the Q-factor of the disk and was measured for very weak coupling to the exciting tapered fiber. Figure 3a shows the results of the measurement of the anti-symmetric mode (coupled disks) of the split TM mode under investigation. The observed doublet in this case is a consequence of the coupling between clockwise and counterclockwise propagating modes in one disk due to Rayleigh scattering at surface roughness. The observed splitting determines the coupling rate Γ_c. Both parameters Γ_0 and Γ_c are obtained by a fit of the measured resonance using (1), (2) and (7) neglecting coupling between the disks and thermal nonlinearity. For an adequate fit we introduce symmetric (s) and antisymmetric (a) standing wave mode amplitudes for a single

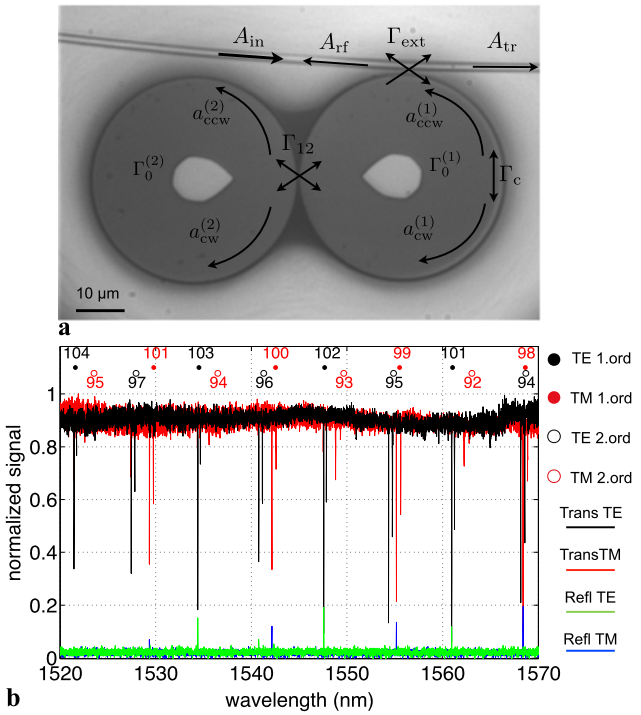

Fig. 2 Microscope image of a two coupled disk sample coupled to a tapered optical fiber (**a**). Highlighted are the relevant variables for the coupled mode model (1) and (2). A measured transmission and reflection spectrum (**b**) of the sample is shown together with calculations obtaining the polarization and mode numbers of the observed first-order (fundamental) and second-order modes

disk resonance (do not be confused with symmetric and anti-symmetric modes of the coupled disk system)

$$a_{s,a} = \frac{1}{\sqrt{2}}(a_{cw} \pm a_{ccw}), \tag{12}$$

in order to decouple the two differential equations (1) and (2) in this particular case. The fit of the measured data in Fig. 3a shows slightly different linewidths $\Delta\lambda_{s,a}$ for both dips, because both standing wave modes have different overlap with the surface of the disk [37], which results in different amount of scattering. For the whole nonlinear system it is easier to deal with the traveling wave mode amplitudes a_{cw} and a_{ccw} where different Q-factors do not make sense. Therefore, and due to the quite small difference of the Q-factors an average value of $Q_0 = 3.6 \times 10^5$ was used for further calculations. This Q-factor corresponds to an energy loss rate $\Gamma_0 = 1.6$ GHz. The splitting of both dips of 7.4 pm is related to a coupling rate of $\Gamma_c = 1.8\Gamma_0$. The resonance frequency mismatch of both disks and the coupling strength can be obtained from the fitting of the two parameters (again neglecting nonlinear terms) to a measurement of the transmission of both symmetric and anti-symmetric modes of the coupled disk system for varying excitation strength (variable taper–disk gap). When the external coupling loss equals the intrinsic loss the transmission drops to zero (critical coupling). While for identical disks the critical coupling occurs at the same external coupling rate for symmetric and anti-symmetric mode, a resonance frequency mismatch of both

Fig. 3 Weak coupled resonance scan with fit to obtain intrinsic loss rate Γ_0 and the coupling ratio between clockwise (cw) and counterclockwise (ccw) propagating mode Γ_c (**a**). From measurement and simulation of both, symmetric and anti-symmetric resonance of the coupled disk system for varying external coupling rate (**b**) the coupling rate between the both disks Γ_{12} as well as their individual resonance mismatch $\Delta\lambda_{12}$ can be obtained. The cw–ccw mode splitting in (**a**) can be clearly seen in the measurement in (**b**) and with the obtained data from (**a**) also in the simulation in (**b**)

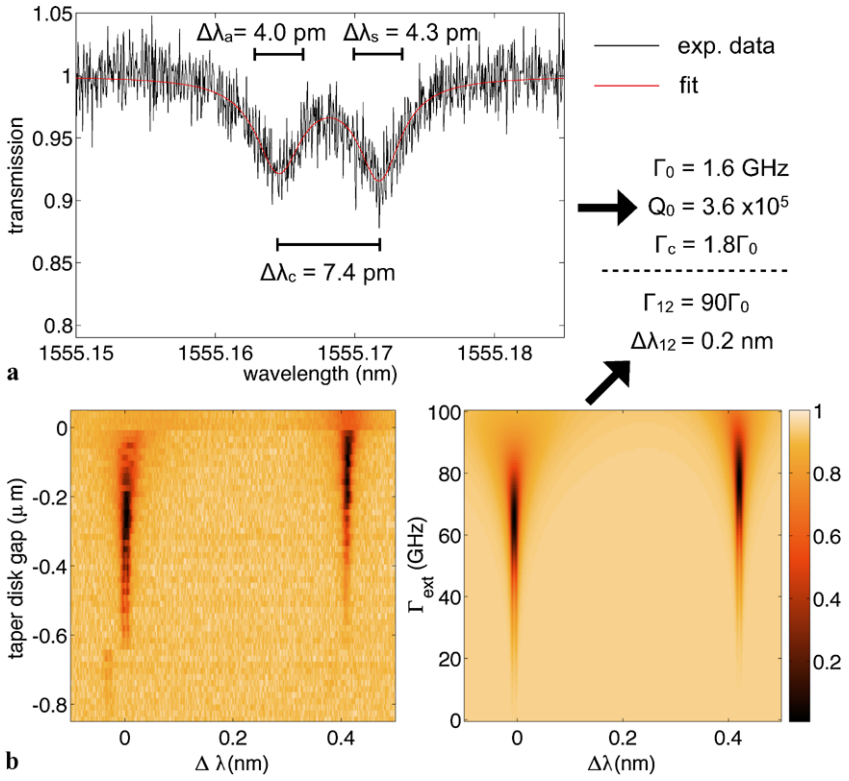

Table 1 Calculation parameters

Parameter	Value	Comments
Material parameters		
Absorption coefficient α	6×10^{-2} m^{-1}	[35]
Material density (fused silica) ρ_0	2.2×10^3 kg m^{-3}	[27]
Thermal conductivity (fused silica) $\bar{k}$	1.4 Wm^{-1} K^{-1}	[38]
Thermal refractivity and expansion β_{th}	4×10^{-6} K^{-1}	[36] and (5)
Heat capacity (fused silica) $\bar{C}$	6.7×10^2 m^2 s^{-2} K^{-1}	[27]
Nusselt number of air *Nu*	0.3	[29]
Single disk parameters		
Disk radius R	20 µm	
Disk thickness d	1.0028 µm	Broad range resonance...
Disk refractive index n	1.4498	...Fit in Fig. 2b
Effective mode volume V_{eff}	6.7×10^{-17} m^3	FEM simulation
Fitted model parameters (linear regime)		
Intrinsic energy loss rate Γ_0	1.6 GHz	Fit in Fig. 3a
Coupling rate cw–ccw-modes Γ_c	2.88 GHz	Fit in Fig. 3a
Coupling rate between disks Γ_{12}	144 GHz	Simulation in Fig. 3b
Resonance mismatch between disks $\Delta\lambda_{12}$	0.2 nm	Simulation in Fig. 3b
Fitted model parameters (non-linear regime)		
Thermal relaxation rate δ_{th}	$10\delta_{\text{th}} = 0.712$ kHz	δ_{th} from (9)
Taper transmission	0.8	Correction factor for P_{in}
Others		
Resonance wavelength (anti-sym. mode) λ_0	1555 nm	TM resonance
Input power P_{in}	0.1 mW ... 4.0 mW	

disks leads to different critical coupling rates. If the second (not directly excited) disk has a resonance at a smaller (larger) wavelength than the directly excited disk, the external coupling rate for critical coupling of the anti-symmetric mode is larger (smaller) than for the symmetric one. Generally, a resonance mismatch of both disks leads to different excitation strengths and stronger splitting of symmetric and anti-symmetric modes. In contrast, the disk separation influences the resonance splitting only. In Fig. 3b the corresponding measurement and simulation are shown, leading to a disk-disk coupling rate of $\Gamma_{12} = 90\Gamma_0$ and a resonance mismatch of $\Delta\lambda_{12} = 0.2$ nm. From a comparison with rigorous calculations the obtained resonance mismatch corresponds to a radius mismatch of the disks of only 3 nm, which is obviously in the range of fabrication accuracy ($\Delta D < 20$ nm).

4.2 Nonlinear characterization

For the nonlinear measurements the spectrum of the coupled disks was recorded for increasing pump power from 0.1 mW up to 4 mW. Due to influences of the transmitted high power on the linearity of the detectors response, the working point was fixed using a variable optical attenuator in front of the detector. Thus far the transmission curves were experimentally normalized, while the reflection signal that is usually much weaker was normalized separately for each pump power. The results for the TM polarized resonance are shown in Fig. 4 for both the symmetric and anti-symmetric modes. For low pump power of 0.1 mW the resonances have symmetric shape, while for a pump power of 4.0 mW the transmission minimum (reflection maximum) shifts toward longer wavelengths with a smooth transition at the short wavelength side and a steep transition at the long wavelength side. This behavior indicates optical bistability due to nonlinear resonance shift that in microresonator systems can be easily visualized by changing the sweeping direction of the tunable laser source [30]. For simulation of this behavior the full system of equations (1), (2), (7), (10) and (11) is used with the parameters listed in Table 1. The results are in agreement with the measured data, especially for the reflected signal. Small discrepancies in the depth of the resonance dips at 4.0 mW pump power are related to fluctuations of the taper-disk coupling during data acquisition. For the high pump power resonance in Fig. 4a an additional calculation was performed with a smaller coupling rate Γ_{ext} leading to better agreement (blue dashed line). The weak splitting of each resonance dip due to coupling of cw

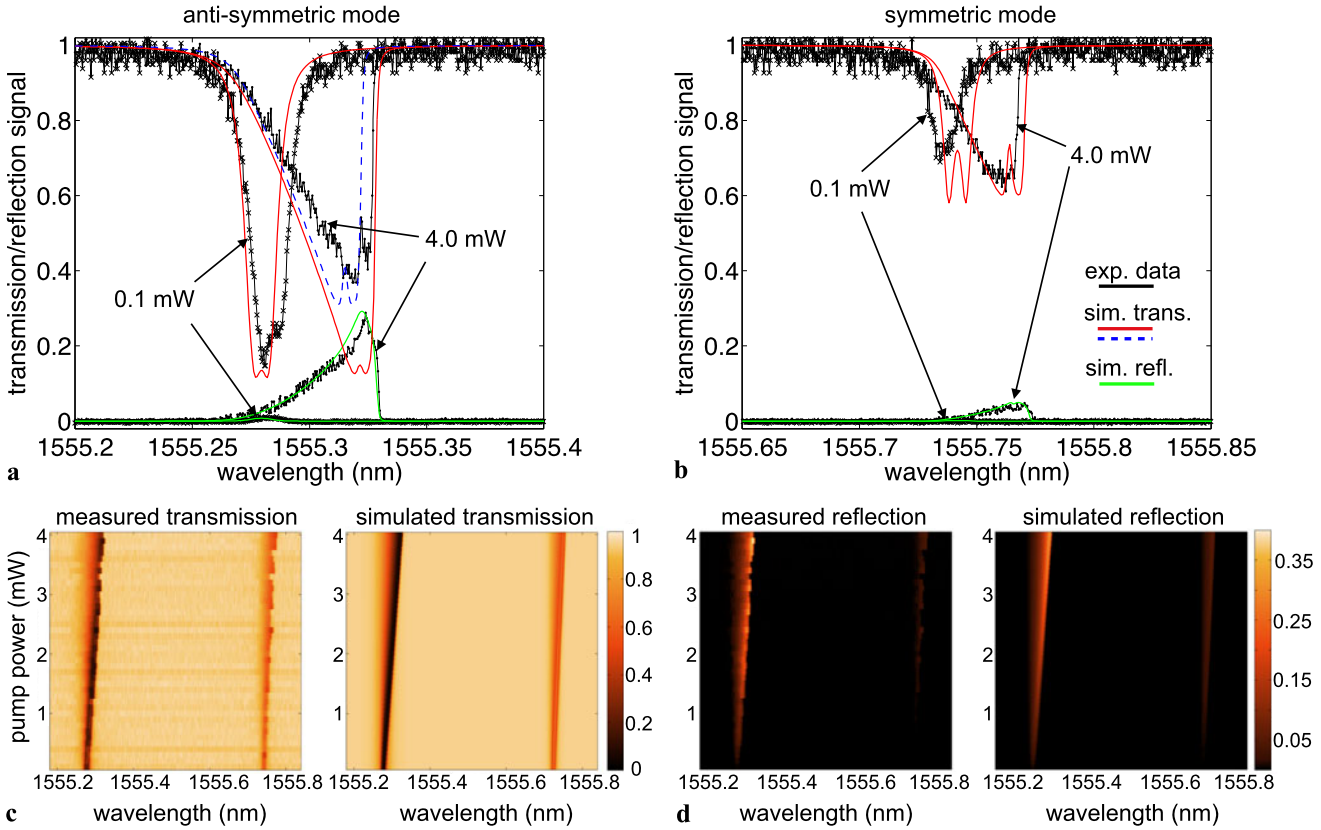

Fig. 4 Spectrum measurement and simulation for anti-symmetric (**a**) and symmetric (**b**) mode of two coupled disks for a pump power of 0.1 mW and 4.0 mW. For 4.0 mW the typical asymmetric resonance shape is observed indicating optical bistability. A comparison of measurement and calculation for both modes over the whole pump power range is shown for transmission (**c**) and reflection (**d**)

and ccw propagating modes in each disk can be observed in the experimental data as well as in the simulations for the strongly excited anti-symmetric mode Fig. 4a only. It is worth noting that in the simulations this weak splitting is symmetric (both tiny dips have the same depth) while in the experiments they do not have the same depth. As it was mentioned in Sect. 4.1 the asymmetric behavior can be modeled by introducing a new basis of eigen modes (12) which can have different Q-factors. The used basis in (1) and (2) is more convenient for coupled disks but it makes no sense to have different Q-factors for cw and ccw mode. For the symmetric mode of the coupled disk system in Fig. 4b this weak splitting was not observed contrary to the simulation. This can be understood by the reduced Q-factor of this modes due to stronger overlap with the rough sidewalls in the coupling region of the disks. The resulting broader resonance dips can hide the weak mode splitting. The agreement of simulation and experimental data over the measured pump power range is shown in Figs. 4c, d.

Besides the described above different normalization for reflection and transmission signals, also considered in the simulations, some additional assumptions made for some of the parameters used in the simulations have to be outlined. According to the transmission losses of the tapered optical fiber a loss of 20 percent was introduced when calculating the input amplitude from the laser output power. As was mentioned in Sect. 2 the thermal relaxation of the disks will strongly influence the nonlinear resonance shift. Depending on the geometry and involved materials either the conductive heat transfer into the substrate or the convective heat transport due to the surrounding gas will dominate. It turned out that in reality a combination of both can lead to an effective relaxation rate in between the usually fast conductive and slow convective ones. Actually, for the presented structure the thermal relaxation rate was found to be $10\delta_{\text{th}}$ (with δ_{th} from (9)) from the best fitting simulations. A detailed view of the transmission and reflection signals is shown in Fig. 5. Due to the different excitation strength of the symmetric and anti-symmetric modes they show a different amount of resonance shift (10 pm/mW for the anti-symmetric mode, 7.5 pm/mW for the symmetric mode). For the transmission one can see a linear shift of the long wavelength tail of the resonances and a relatively steep transition, whereas for the short wavelength side the transition gets smoother as stronger the shift is, leading to a slightly bend curve for a fixed transmission value (dot-

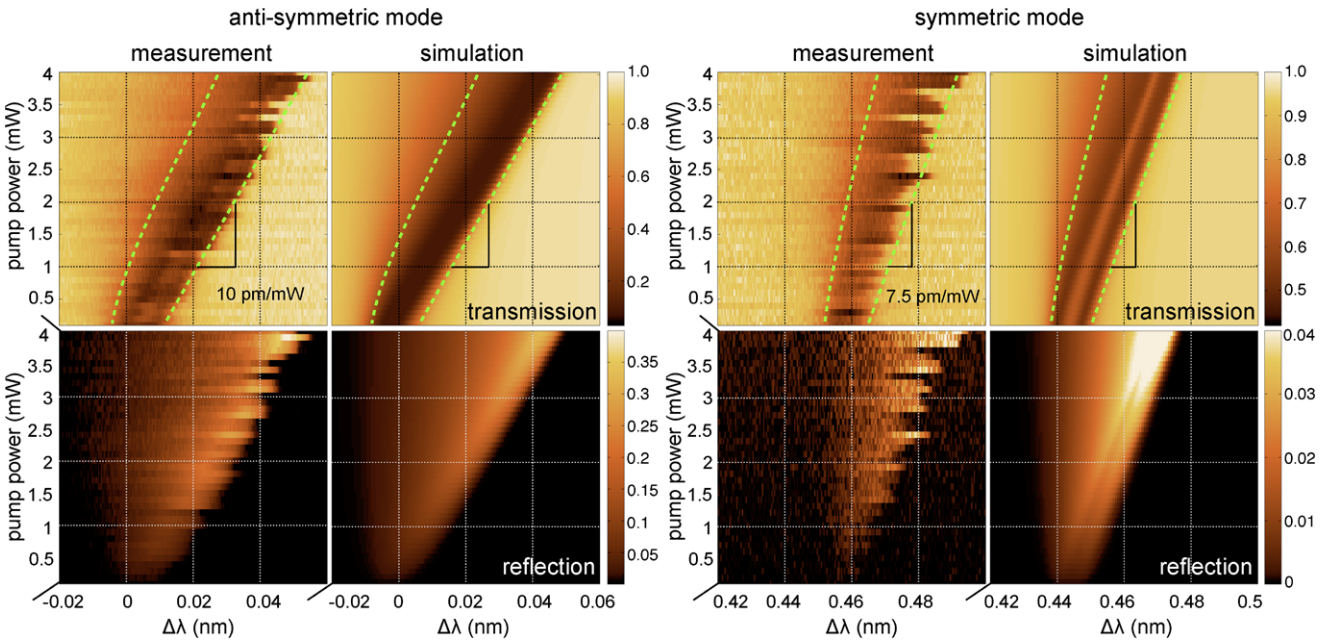

Fig. 5 Detailed view on nonlinear reflection and transmission measurements and simulations

ted lines in Fig. 5). The reflection signals show the same transition behavior for both tails of the resonance but due to the weak maximum signal the details of the short wavelength side are much clearer. For the weak excited symmetric resonance the reflection signal is close to the noise level of the detector leading to significant deviations between experiment and simulation. Nevertheless, the amount of resonance shift as well as the maximum reflection signal is reproduced by the calculations. As a further indication of the reliability of the used nonlinear coupled mode model the obtained temperature changes of the mode volume can be calculated from (7). For the highest pump power of 4 mW a temperature difference $\Theta^{(1)}$ of the excited (first) disk of 8.46 K was obtained. For the not directly excited (second) disk $\Theta^{(2)} = 4.63$ K was calculated. Both values are in agreement with results obtained for a comparable fused silica microresonator [39].

In conclusion a detailed analysis of temperature induced nonlinear resonance shift in two coupled disk microresonators was presented. The experimental results are in good agreement with the theoretical calculations based on coupled mode theory including thermal nonlinearity. Individual slopes of resonance shift with increasing pump power can be observed for distinct eigenstates of coupled disk systems due to differences in the excitation strength. These differences are related to a size mismatch of the individual disks in the coupled system. The calculated size mismatch of the coupled disks of only 3 nm emphasizes the challenging fabrication tolerances that have to be fulfilled for the realization of working samples of coupled disk structures. Although a manipulation of the individual disks after fabrication is possible to obtain resonance matching, it will complicate the whole measurement setup and procedure and might not be useful for larger arrangements of coupled disks. The observed optical coupling of disk microresonators is promising for further studies of more complex structures involving larger number of disks also in two-dimensional configurations in the framework of spatio-temporal dynamics in discrete optical systems. As it was shown in the paper the fabrication of such structures is possible. Beside this study of fundamental physical processes coupled microresonators might be useful for optical filter applications and laser stabilization. The observed difference in the resonance shifts can be used for tunable filter applications with variable spacing of filter wavelengths depending on the applied input power.

Acknowledgements We gratefully acknowledge funding of this work by the Deutsche Forschungsgemeinschaft (DFG) within the research unit 532.

References

1. V.B. Braginsky, M.L. Gorodetsky, V.S. Ilchenko, Phys. Lett. A **137**, 393 (1989)
2. S.L. McCall, A.F.J. Levi, R.E. Slusher, S.J. Pearton, R.A. Logan, Appl. Phys. Lett. **60**, 289 (1992)
3. V.S. Ilchenko, M.L. Gorodetsky, X.S. Yao, L. Maleki, Opt. Lett. **26**, 256 (2001)
4. V.S. Ilchenko, A.B. Matsko, IEEE J. Sel. Top. Quantum Electron. **12**, 15 (2006)
5. H.B. Lin, A.L. Huston, J.D. Eversole, A.J. Campillo, J. Opt. Soc. Am. B **7**, 2079 (1990)
6. S.M. Spillane, T.J. Kippenberg, K.J. Vahala, Nature **415**, 621 (2002)

7. T.J. Kippenberg, S.M. Spillane, K.J. Vahala, Phys. Rev. Lett. **93**, 83904 (2004)
8. V.B. Braginsky, Y.I. Vorontsov, K.S. Thorne, Science **209**, 547 (1980)
9. S.M. Spillane, T.J. Kippenberg, K.J. Vahala, K.W. Goh, E. Wilcut, H.J. Kimble, Phys. Rev. A **71**, 013817 (2005)
10. T.J. Kippenberg, K.J. Vahala, Science **321**, 1172 (2008)
11. L.I. Deych, C. Schmidt, A. Chipouline, T. Pertsch, A. Tunnermann, Phys. Rev. A **77**, 051801(R) (2008)
12. Z. Chen, A. Taflove, V. Backman, Opt. Lett. **31**, 389 (2006)
13. L.I. Deych, O. Roslyak, Phys. Rev. E **73**, 036606 (2006)
14. L.I. Deych, C. Schmidt, A. Chipouline, T. Pertsch, A. Tünnermann, Appl. Phys. B **93**, 21 (2008)
15. Y. Hara, T. Mukaiyama, K. Takeda, M. Kuwata-Gonokami, Phys. Rev. Lett. **94**, 203905 (2005)
16. A. Naweed, G. Farca, S.I. Shopova, A.T. Rosenberger, Phys. Rev. A **71**, 43804 (2005)
17. S.P. Ashili, V.N. Astratov, E.C.H. Sykes, Opt. Express **14**, 9460 (2006)
18. K. Totsuka, N. Kobayashi, M. Tomita, Phys. Rev. Lett. **98**, 213904 (2007)
19. V.N. Astratov, J.P. Franchak, S.P. Ashili, Appl. Phys. Lett. **85**, 5508 (2004)
20. B.M. Möller, U. Woggon, M.V. Artemyev, Phys. Rev. B **75**, 245327 (2007)
21. S. Boriskina, J. Opt. Soc. Am. B **23**, 1565 (2006)
22. E.I. Smotrova, A.I. Nosich, T.M. Benson, P. Sewell, IEEE J. Sel. Top. Quantum Electron. **12**, 78 (2006)
23. A. Yariv, Y. Xu, R.K. Lee, A. Scherer, Opt. Lett. **24**, 711 (1999)
24. J.K.S. Poon, J. Scheuer, Y. Xu, A. Yariv, J. Opt. Soc. Am. B **21**, 1665 (2004)
25. A.A. Savchenkov, V.S. Ilchenko, A.B. Matsko, L. Maleki, IEEE Photonics Technol. Lett. **17**, 136(2005)
26. C. Schmidt, A. Chipouline, T. Käsebier, E.-B. Kley, A. Tünnermann, V. Shuvayev, L.I. Deych, T. Pertsch, Phys. Rev. B **80**, 043841 (2009)
27. I.S. Grudinin, K.J. Vahala, Opt. Express **17**, 14088 (2009)
28. N. Ahkmediev, A. Ankiewicz, *Dissipative Solitons* (Springer, Berlin, 2005)
29. V.S. Ilchenko, M.L. Gorodetsky, Laser Phys. **2**, 1004 (1992)
30. C. Schmidt, A. Chipouline, T. Pertsch, A. Tünnermann, O. Egorov, F. Lederer, L.I. Deych, Opt. Express **16**, 6285 (2008)
31. A.I. Nosich, E.I. Smotrova, S.V. Boriskina, T.M. Benson, P. Sewell, Opt. Quantum Electron. **39**, 1253 (2007)
32. J.C. Knight, G. Cheung, F. Jacques, T.A. Birks, Opt. Lett. **22**, 1129 (1997)
33. S.M. Spillane, T.J. Kippenberg, O.J. Painter, K.J. Vahala, Phys. Rev. Lett. **91**, 43902 (2003)
34. H.A. Haus, *Waves and Fields in Optoelectronics* (Prentice Hall, New York, 1984)
35. A.E. Fomin, M.L. Gorodetsky, I.S. Grudinin, V.S. Ilchenko, J. Opt. Soc. Am. B **22**, 459 (2005)
36. C. Schmidt, A. Chipouline, T. Käsebier, E.-B. Kley, A. Tünnermann, T. Pertsch, Opt. Lett. **35**, 3351 (2010)
37. M. Borselli, T.J. Johnson, O. Painter, Opt. Express **13**, 1515 (2005)
38. R.W. Boyd, *Nonlinear Optics* (Academic Press, London, 2003)
39. T. Carmon, L. Yang, K.J. Vahala, Opt. Express **12**, 4742 (2004)